Polymer Journal (2019) 51:845–850
https://doi.org/10.1038/s41428-019-0198-z

ORIGINAL ARTICLE

Visco- and plastoelastic fracture of nanoporous polymer sheets

Takako Tomizawa[1] · Ko Okumura[1]

Received: 7 January 2019 / Revised: 23 March 2019 / Accepted: 25 March 2019 / Published online: 9 May 2019

Abstract

We study the dependence of the fracture surface energy on the pulling velocity for nanoporous polypropylene (PP) sheets to identify two components: static and dynamic components. We show that these terms can be interpreted, respectively, as plastoelastic and viscoelastic components, as has been shown for soft polyethylene (PE) foams in previous work. Considering significant differences in the pore size, volume fraction, and Young's modulus of the present PP and previous PE sheets, the present results suggest a universal physical mechanism for the fracture of porous polymer sheets. The simple physical interpretation emerging from the mechanism could be useful for developing tough polymers. Equivalence of Griffith's energy balance in fracture mechanics to a stress criterion is also discussed and demonstrated using the present experimental data.

Introduction

Cellular solids, which are porous materials with well-defined pore sizes, are found in natural and artificial materials and are a useful form of materials [1]. Cork, balsa, and apples [2] are cellular solids originated from plants, and the stereom of echinoderms [3], the skeleton of a certain sponge [4], and the frustle of diatoms [5] are examples from other living creatures. Such materials possess mechanical advantages because they can be light, strong, shock absorbing, and heat retaining. Accordingly, active studies have been performed on mechanical and fracture mechanical properties, focusing on an important parameter for cellular solids, the volume fraction of the matrix material ϕ [1]. However, studies on velocity-dependent properties of their fracture are relatively limited compared with intensive studies that have been performed on other materials such as adhesive [6–10], laminar [11], viscoelastic [12, 13], weakly cross-linked [14, 15], biopolymer gel [16], and biological composite [17] materials, including recent active experimental [18–22], numerical [23–26], and theoretical [27, 28] studies [29] on the velocity jump in crack propagation in polymer sheets.

Previously, we studied mechanical and fracture mechanical properties of soft solidified foam of noncross-linked polyethylene. Young's modulus E, the characteristic pore size d_0, and the volume fraction ϕ of the foams were on the orders of 1 MPa, 1 mm, and 0.03, respectively. For the soft foams, we established scaling laws for Young's modulus and the fracture surface energy as a function of ϕ. The scaling laws thus found are different from the laws established for well-studied hard cellular solids of Young's modulus typically 3000 MPa [30]. Furthermore, we revealed for the same soft solidified foams a simple relation between the fracture surface energy (required at the crack initiation) and the pulling velocity with a clear physical interpretation [31]. Here, we test this simple description for the velocity dependence of the fracture energy using a porous polymer of different nature. This sample is not polyethylene (PE) but polypropylene (PP) and E, d_0, and ϕ in this case are significantly different from those in the previous study: $E \sim 200$ MPa, $d_0 \sim 1$ μm, and $\phi \sim 0.5$. As a result, we found that the same description is well-applicable for this quite different material and suggest that the simple description proposed in the previous study can be universally relevant to a certain class of porous polymers.

Experimental section

Materials

In this experiment, we use sheets of polypropylene (PP) that possess a porous structure, as shown in Fig. 1a. The structure may be characterized by a few different length

✉ Ko Okumura
okumura@phys.ocha.ac.jp

[1] Department of Physics, Ochanomizu University, Tokyo, Japan

scales and the largest scale is around 1 μm, which could be comparable with 10^{-5} m, as seen from the SEM image. The volume fraction ϕ and the thickness of the sheet are 0.44 and 23 μm, respectively. The sheet is fabricated from bulk with a stretching process and, thus, tends to be stronger in the direction defined as the machine direction.

Mechanical measurement

The elongation of a sheet from the natural length and the tensile force acting on the sheet were measured with a hand-made setup used in our previous study [31]. This setup is equipped with horizontally placed two pairs of clamp bars specially designed for sheet samples of a dimension comparable with 50 cm to avoid any slips at the clamps and local slacking of a sheet sample under stretch. The horizontal width of the sample is 10 cm for failure stress measurements (5 cm for force-extension measurements) and the vertical height (i.e., the distance between the inner edges of the clamp bars) is 12.5 cm. The bottom pair of clamp bars are fixed to the setup frame, while the position and speed of the mobile upper pair of clamp bars can be controlled by a slider system (EZSM6D040 K, Oriental Motor) through a digital force gauge (FCC-50B, NIDEC-Shimpo). Each measurement is made for a given fixed velocity of the upper clamp, which defines the pulling velocity V. All experiments are performed by setting the machine direction in horizontal direction, and the constant stretching speed V is given in the vertical direction by the controlled slider system. The pulling velocity V is varied from 0.03 mm/s to 0.4 mm/s.

Fracture mechanical measurements are performed with the same setup but by introducing a macroscopic line crack with a sharp knife at the center of the sample (see Fig. 1b). The line crack is created in the horizontal direction (i.e., the machine direction), and the length $2a$ is varied from 2 to 32 mm.

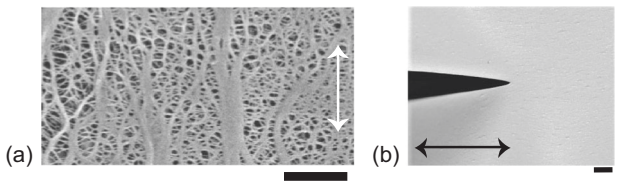

Fig. 1 **a** An SEM image of the porous polypropylene sheet used in the experiment (Copyright 2018 by Mitsubishi Chemical Corporation). The length of the scale bar is 1 μm. **b** Magnified view near a crack tip. The machine direction are shown by double-headed arrows, which is perpendicular to the pulling direction. The length of the scale bar is 1 mm

Results

Stress–strain curve and Young's modulus

Figure 2a shows typical results of the relation between stress σ and strain ε of a sheet sample at different velocities. The nearly overlapped two sets of data at each velocity show high reproducibility of the experiment. The relation exhibits a nonlinear response with a weak dependence on velocity. However, in the initial regime in which ε and σ are less than ~0.01 and ~2 MPa, respectively, the relation is almost linear and is almost independent of velocity (see Fig. 2a' for the magnified version). In fact, Young's modulus extracted from this region is approximately constant, as shown in Fig. 2b. Here, the modulus at each velocity is determined as the average of the three moduli obtained from the initial regimes of three sets of force-elongation measurements performed at each velocity, with the bottom and top values of each error bar showing the minimum and maximum of the three results.

Failure stress of a sample with a line crack and fracture surface energy

Figure 3a and b shows typical results for the relation between the failure stress σ_f and the half-length of the line crack a. σ_f for given a and V are measured three times, and

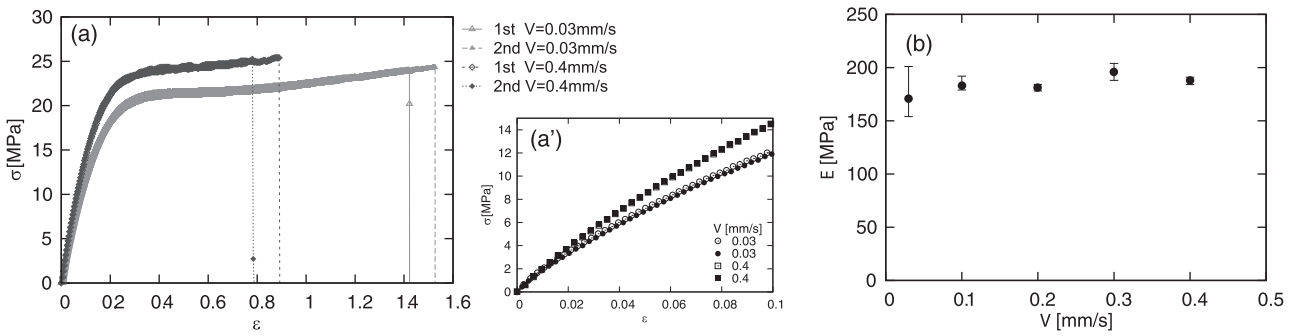

Fig. 2 **a** Stress–strain curves obtained from the force-extension measurements performed with samples without any macroscopic cracks at extension velocities of $V = 0.03$ and 0.4 mm/s. **a'** Magnified version of **a** to more clearly show the initial quasi-linear regime. **b** Young's modulus E determined in the initial regime in the stress–strain curve as a function of the stretching velocity V

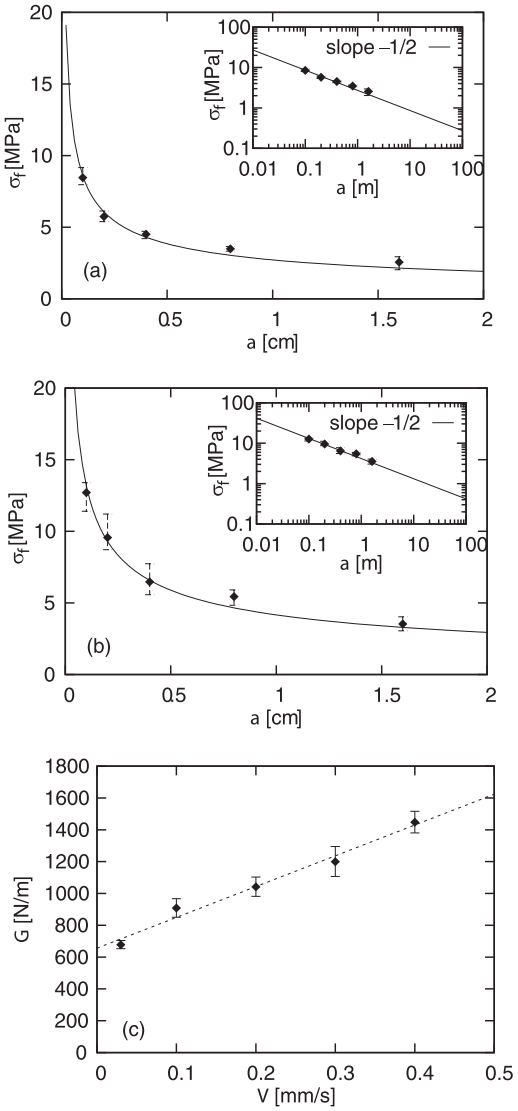

Fig. 3 Failure stress σ_f as a function of crack size $2a$ at $V = 0.03$ mm/s (**a**) and $V = 0.4$ mm/s (**b**). The insets show corresponding plots on a log–log scale. **c** Fracture surface energy G as a function of velocity V

the average of the three values is plotted with an error bar in the figure. When data are plotted on a log–log scale, the data for a given V clearly collapse on a straight line with slope $-1/2$. This justifies that we use the following Griffith's formula to estimate the fracture surface energy G for a given V [32]:

$$\sigma_f = \left(\frac{2EG}{\pi a}\right)^{1/2} \tag{1}$$

Figure 3c shows the relation between the pulling velocity V and the fracture surface energy G on the basis of Eq. (1). The relation can be well described by the linear form: $G = A + BV$. Here, A and B are constants independent of V. On the other hand, it is theoretically justified and experimentally confirmed that G is proportional to the volume fraction ϕ [30, 31]. Exploiting this property, we rewrite the expression $G = A + BV$ in the following form:

$$G = \phi G_0(1 + V/V_0) \tag{2}$$

with the introduction of G_0 and V_0, which are independent of V (G_0 and V_0 are defined by the relations $A = \phi G_0$ and $B = \phi G_0/V_0$).

In the following, we justify that the above expression can be reasonably well interpreted as in the following form:

$$G = \phi(\sigma_Y + \eta(V/d))\delta \tag{3}$$

We examine the validity of the above expression at the level of scaling laws. For simplicity, we regard $\phi \sim 1$ and ignore this factor in the following. The first term $\phi\sigma_Y\delta \sim \sigma_Y\delta$ can be regarded as the standard expression for plastic fracture, where σ_Y is the yield stress, and δ is the crack-opening distance [32]. Considering a typical value of σ_Y for PP, say, 50 MPa (this estimate is consistent, at a semi-quantitative level, with Fig. 2a, if we remind that $\phi = 0.44$), the opening distance δ can be estimated as $\sim 10^{-5}$ m because $\phi G_0 \sim G_0$ ($\sim\sigma_Y\delta$) is estimated as 650 J/m^2 from Fig. 3c. This value of δ is comparable with the largest characteristic scale of the porous structure in the sample; it is quite natural that we expect the crack-opening distance scale as this length scale. The second term, in particular, the quantity $\eta(V/d)$ just describes the viscous stress that we have to add to σ_Y in the dynamic case. Here, d describes the length scale around the crack tip dynamically affected, and it is natural to assume that this scale as δ. Taking the viscous effect into account is reasonable because the glass transition temperature of PP (typically 0 °C) is well below ambient temperature at which the experiments were performed, and the viscosity η is estimated as 2×10^6 Pa.s from Fig. 3c by estimating the value $\phi G_0/V_0 \sim G_0/V_0$, which scale as $\eta\delta/d \sim \eta$. To gain physical insight, we can roughly estimate the number of monomers N in the entangled polymer by invoking the reptation model [33]. This crude estimate gives $\eta \sim \eta_0 N^3/N_e^2$ with N_e as the entangle distance (~100) and η_0 as the viscosity of monomers (~1 mPa.s). As a result, we obtain a plausible value, $N \sim 10^4$. Since we have established the same reasoning for Eq. (3) in ref. [31] for soft foam sheets of polyethylene, this result suggests a certain degree of universality of Eq. (3). Our result suggests that the dynamic toughness is significantly increased if the number of monomers N is increased, because the velocity-dependent term in G contains the viscosity η and, even if the reptation model is not appropriate, η is strongly dependent on N.

Equation (3) established as above can be interpreted as composed of a static term reflecting a plastoelastic effect and a dynamic term reflecting a viscoelastic effect, as

explained as follows. This expression is composed of two terms, one independent of V and the other dependent on V. In other words, G is composed of the static and dynamic parts. The static part reflects a plastic effect because it is proportional to the yield stress σ_Y. The dynamic part corresponds to the viscous effect because it originates from viscous stress. On the other hand, G in this study is determined by linear-elastic fracture mechanics. Therefore, it is natural to interpret the static and dynamic terms as plastoelastic and viscoelastic effects, respectively.

Equivalence of Griffith energy balance to a stress criterion

As we discussed in our previous paper, the energy balance is equivalent to a stress criterion, if we note that the stress concentration is cutoff at the length scale below which the continuum description fails, although Griffith's energy balance is sometimes distinguished from the stress criteria for fracture. (This cutoff length scale corresponds to the largest scale characterizing the porous structure and, thus, will be called d in the following.) This can be experimentally confirmed for the present material. To illustrate this, let us briefly review how the energy balance reduces to a stress criterion. We introduce a critical failure stress σ_c for a given material through the following relation:

$$\sigma_c \simeq (EG/d)^{1/2} \tag{4}$$

This equation comes from the well-known Griffith's formula for the failure stress $\sigma_f \simeq (EG/a)^{1/2}$ for a crack of length $\sim a$ and the idea of Griffith's cavities. We further introduce the maximum stress that appears at the crack tip at the critical point of failure at which the remote stress σ_0 is equal to the failure stress σ_f:

$$\sigma_m \simeq \sigma_f (a/d)^{1/2} \tag{5}$$

This equation comes from the well-known Inglis' stress concentration formula for the stress distribution around a crack $\sigma(r) \simeq \sigma_0 (a/r)^{1/2}$ at a distance r from the crack tip, which should be cutoff at the scale d. (This relation $\sigma(r) \simeq \sigma_0 (a/r)^{1/2}$ was confirmed in numerical studies [34, 35] and Eq. (5) was directly confirmed in another numerical study [36].) The stress criteria that is equivalent to Griffith's energy balance is then given by

$$\sigma_c \simeq \sigma_m \tag{6}$$

In fact, from Eqs. (4)–(6), we recover Griffith's formula.

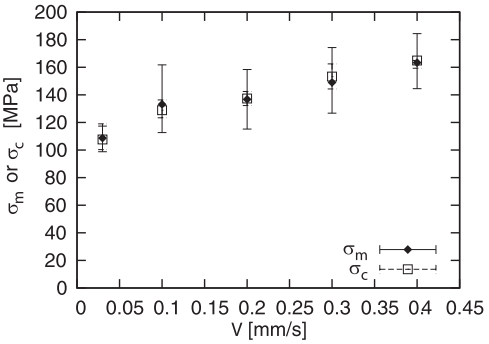

Fig. 4 σ_c vs. σ_m. See the text for the details

To confirm that the above description is relevant to the present experimental data, we experimentally determine σ_c and σ_m, respectively, from Eq. (4) (using measured values of E, G, and d) and from Eq. (5) (using measured values of σ_f, a, and d). We here set the coefficient for Eq. (4) to be 1 and that for Eq. (5) to be 0.841, and we use $d = 10^{-5}$ m for both equations, for simplicity. The results are shown in Fig. 4, which confirms that the stress criteria Eq. (6) is satisfied for the experimentally observed fractures and, thus, the above description is consistent with our experimental results. (If we denote dimensionless numerical coefficients suppressed in Eqs. (4)–(6) as c_4, c_5, and c_6, respectively, Eq. (6) can be expressed as $(EG/d)^{1/2} = (c_6 c_5/c_4)\sigma_f (a/d)^{1/2}$, which means that the agreement between σ_c an σ_m in Fig. 4 shows that $c_6 c_5/c_4$ is close to 0.841).

Conclusion

We studied the fracture surface energy at the onset of crack initiation as a function of the pulling velocity. As a result, we find that the fracture energy is described by static and dynamic components. The former corresponds to the standard plastic fracture, and the latter reflects the viscous flow that occurs at a crack tip. The both components are characterized by the length scale, which is comparable with the pore size. The existence of the dynamic and viscous components suggests a simple principle for toughening: the increase in the degree of polymerization could greatly enhance the dynamic toughness. The equivalence of Griffith's energy balance to a stress criterion is also demonstrated. These results parallel the results obtained for significantly different porous polymer sheets, which suggests the universality of the present physical interpretation, although further studies will be needed to clarify the limitations of the present interpretation.

Considering that the basic physical properties of polymer materials are quite dependent on preparation crystallinity, molecular orientation, the size and shape of the porous

structure, and the types of polymers [37], the emergence of this kind of universality may be unexpected. (The fracture of crystalline polymers on microscopic scales are starting to be reproduced in simulations [38]). We consider that one of the reasons for this universality comes from the introduction of a macroscopic crack, whose scale is much larger than characteristic scales for crystallinity, the domains in which the molecules are oriented, the porous structure, and so on. On such a macroscopic scale, it is known that polymers universally exhibit yielding and viscous flow in a similar manner. When these points are considered, it would not be surprising if the fracture associated with a macroscopic crack is universally governed by yielding and viscous flow of their simplest forms, which we suggest here.

The study concerns the fracture surface energy required at the onset of crack initiation. Such a fracture energy should be in general distinguished from the fracture energy required during crack propagation. In fact, we recently studied the relation between the energy release rate, which can be interpreted as the fracture surface energy required during crack propagation, and the crack-propagation velocity, using the same material studied in this study [21]. As a result, we did not observe crack propagation in the velocity range studied in this study. However, in the previous study [21], for a technical reason, the constant-speed crack propagation with a fixed-grip condition was initiated some time after we applied a given strain to samples, and we consider that the effect of stress relaxation due to this preparation time could suppress crack propagation. This point will be further discussed elsewhere [22].

Acknowledgements The authors are grateful to the Mitsubishi Chemical Corporation for providing nanoporous sheet samples and the SEM image shown in Fig. 1a. The authors thank Dr. Atsushi Takei for technically helping them for experiments. This work was partly supported by ImPACT Program of Council for Science, Technology and Innovation (Cabinet Office, Government of Japan).

Compliance with ethical standards

Conflict of interest The authors declare that they have no conflict of interest.

References

1. Gibson LJ, Ashby MF. Cellular solids: structure and properties. Cambridge, UK: Cambridge University Press.; 1999.
2. Khan ALIA, Vincent JFV. Mechanical damage induced by controlled freezing in apple and potato. J Texture Stud. 1996;27:143–57.
3. Emlet RB. Echinoderm calcite: a mechanical analysis from larval spicules. Biol Bull. 1982;163:264–75.
4. Aizenberg J, Weaver JC, Thanawala MS, Sundar VC, Morse DE, Fratzl P. Skeleton of euplectella sp.: structural hierarchy from the nanoscale to the macroscale. Science. 2005;309:275–8.
5. Hamm CE, Merkel R, Springer O, Jurkojc P, Maier C, Prechtel K, et al. Architecture and material properties of diatom shells provide effective mechanical protection. Nature. 2003;421:841–3.
6. Gent AN, Schultz J. Effect of wetting liquids on the strength of adhesion of viscoelastic material. J Adhes. 1972;3:281–94.
7. Chaudhury MK. Rate-dependent fracture at adhesive interface. J Phys Chem B. 1999;103:6562–6.
8. Morishita Y, Morita H, Kaneko D, Doi M. Contact dynamics in the adhesion process between spherical polydimethylsiloxane rubber and glass substrate. Langmuir. 2008;24:14059–65.
9. Creton C, Kramer E, Brown H, Hui C-Y. Adhesion and fracture of interfaces between immiscible polymers: from the molecular to the continuum scal. Adv Polym Sci. 2002;156:53–136.
10. Bhuyan S, Tanguy F, Martina D, Lindner A, Ciccotti M, Creton C. Crack propagation at the interface between soft adhesives and model surfaces studied with a sticky wedge test. Soft Matter. 2013;9:6515–24.
11. Kinloch AJ, Lau CC, Williams JG. The peeling of flexible laminates. Int J Fract. 1994;66:45–70.
12. Greenwood JA, Johnson KL. The mechanics of adhesion of viscoelastic solids. Philos Mag A. 1981;43:697–711.
13. Schapery RA. A theory of crack initiation and growth in viscoelastic media. Int J Fract. 1975;11:141–59.
14. de Gennes PG. C R Acad Sci Paris, t. Serie II. 1988;307:1949–53.
15. Saulnier F, Ondarcuhu T, Aradian A, Raphaël E. Adhesion between a viscoelastic material and a solid surface. Macromolecules. 2004;37:1067–75.
16. Lefranc M, Bouchaud E. Mode i fracture of a biopolymer gel: rate-dependent dissipation and large deformations disentangled. Extrem Mech Lett. 2014;1:97–103.
17. Bouchbinder E, Brener EA. Viscoelastic fracture of biological composites. J Mech Phys Solids. 2011;59:2279–93.
18. Tsunoda K, Busfield JJC, Davies CKL, Thomas AG. Effect of materials variables on the tear behaviour of a non-crystallising elastomer. J Mater Sci. 2000;35:5187–98.
19. Morishita Y, Tsunoda K, Urayama K. Velocity transition in the crack growth dynamics of filled elastomers: contributions of nonlinear viscoelasticity. Phys Rev E. 2016;93:043001.
20. Morishita Y, Tsunoda K, Urayama K. Crack-tip shape in the crack-growth rate transition of filled elastomers. Polymer. 2017;108:230–41.
21. Takei A, Okumura K. Crack propagation in porous polymer sheets with different pore sizes. MRS Communications. 2018; p. 1–6. https://doi.org/10.1557/mrc.2018.222.
22. Tomizawa T, Okumura K. Velocity jump in the crack propagation induced on a semi-crystalline polymer sheet by constant-speed stretching. Polymer. 2019 (in press).
23. Kubo A, Umeno Y. Velocity mode transition of dynamic crack propagation in hyperviscoelastic materials: a continuum model study. Sci Rep. 2017;7:42305.
24. Aoyanagi Y, Okumura K. Stationary crack propagation in a two-dimensional visco-elastic network model. Polymer. 2017;120:94–9.
25. Aoyanagi Y, Okumura K. Crack propagation in nonlinear viscoelastic models. Macromol. 2019; under review.
26. Aoyanagi Y, Okumura K. Crack propagation under static and dynamic boundary conditions. Polymer. 2019; under review.
27. Sakumichi N, Okumura K. Exactly solvable model for a velocity jump observed in crack propagation in viscoelastic solids. Sci Rep. 2017;7:8065.
28. Okumura K. Velocity jumps in crack propagation in elastomers: Relevance of a recent model to experiments. J Phys Soc Jpn. 2018;87:125003.

29. Kubo A, Sakumichi N, Morishita Y, Okumura K, Tsunoda K, Urayama K et al. Dynamic glass transition dramatically accelerates crack propagation in rubber-like solids. Sci Rep. 2019; under review.
30. Shiina Y, Hamamoto Y, Okumura K. Fracture of soft cellular solids - case of non-crosslinked polyethylene foam. Europhys Lett. 2006;76:588–94.
31. Kashima Y, Okumura K. Fracture of soft foam solids: interplay of visco-and plasto-elasticity. ACS Macro Lett. 2014;3:419–22.
32. Anderson TL. Fracture mechanics. 3rd ed. Boca Raton, Florida: CRC Press; 2005.
33. De Gennes PG. Scaling concepts in polymer physics. Ithaca, NY: Cornell University Press; 1979.
34. Nakagawa S, Okumura K. Crack-tip stress concentration and mesh size in networks. J Phys Soc Jpn. 2007;76:4801.
35. Aoyanagi Y, Okumura K. Crack-tip stress concentration and structure size in nonlinear structured materials. J Phys Soc Jpn. 2009;78:034402.
36. Murano M, Okumura K. Simple Network Model for Reinforcement of Materials with Voids, J. Phys. Soc. Jpn. 2014;83:035001.
37. Strobl GR, Strobl GR. The physics of polymers, 2nd Ed. (Springer-Verlag Berlin; 1997).
38. Higuchi Y. Fracture processes of crystalline polymers using coarse-grained molecular dynamics simulations. Polymer J, 2018;50:579–88.